THE JOURNAL OF PHYSICAL CHEMISTRY B

ARTICLE

pubs.acs.org/JPCB

Photoinduced Charge Separation in an Organic Donor−Acceptor Hybrid Molecule

Aliaksandr Marchanka,[†] Stefan K. Maier,[‡] Sigurd Höger,[‡] and Maurice van Gastel*[,†,§]

[†]Institut für Physikalische und Theoretische Chemie, Rheinische Friedrich-Wilhelms-Universität Bonn, Wegelerstrasse 12, D-53115 Bonn, Germany

[‡]Kekulé-Institut für Organische Chemie und Biochemie, Rheinische Friedrich-Wilhelms-Universität Bonn, Gerhard-Domagk-Strasse 1, D-53121 Bonn, Germany

Supporting Information

ABSTRACT: Photoinduced charge separation in blends of organic materials of different electronic affinity and in organic donor−acceptor hybrids is a process of increasing importance for biological and artificial energy conversion and photovoltaics. Organic polymer solar cells are composed of an electron donor and an electron acceptor between which an electron transfer occurs after excitation by sunlight. Charge separation results in the formation of donor cation radicals and acceptor anion radicals. Here, we present our studies on a donor−acceptor hybrid molecule composed of a phenylene−bithiophene macrocycle used as a donor and a perylene bisimide acceptor. Using continuous wave EPR and modern pulsed EPR methodology in combination with light excitation, intermolecular as well as intramolecular charge separation has been observed. Light-induced charge separation observed upon selective excitation of either one of the chromophores indicates that both LUMO-based and HOMO-based electron transfer from donor to acceptor takes place. These experimental findings are corroborated by DFT calculations in which the HOMO of the donor−acceptor hybrid molecule is found at the phenylene−bithiophene macrocycle and the LUMO at the perylene bisimide.

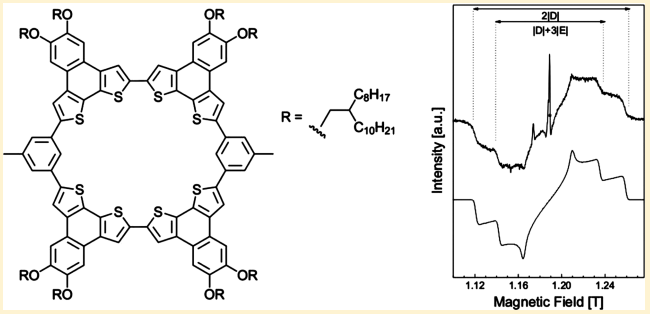

INTRODUCTION

The increased demand for energy in the form of electricity requires devices making use of renewable energy sources like wind, water, or solar energy. The conversion of sunlight into electricity by solar cells is a very attractive alternative to classical energy sources, and the production of solar cells has advanced considerably in recent years.[1] Solar energy conversion based on organic solar cells is a relatively novel technology with the prospect of inexpensive large-scale production.[2] Energy conversion efficiencies achieved to date using conductive polymers are low as compared to inorganic materials,[3] but its growth is rapid and an energy conversion efficiency of more than 8% has recently been reached.[4]

Conjugated polymers are increasingly used for the fabrication of electronic and optoelectronic devices like photovoltaic (PV) elements. Organic polymer solar cells are composed of an electron donor (D) and an electron acceptor (A) layer in which an electron transfer occurs after light-induced excitation of the donor component resulting in the formation of donor cation radicals and acceptor anion radicals. A breakthrough in realizing an efficient conversion of solar energy into electrical energy has been achieved by using a phase-separated blend of electron donor and electron acceptor materials.[5] Because photoinduced electron transfer from nondegenerate ground-state conjugated polymers to fullerenes has been discovered,[6−9] these materials have become of increasing interest for the production of flexible large area solar cells and photodetectors.

Organic electron donor materials are mostly based on poly(phenylenevinylenes) (PPVs), oligo- or polythiophenes (e.g., poly(3-hexylthiophene) (P3HT), polymers based on fused ring systems (like cyclopentadithiophenes or dithienopyrroles), or condensed polycyclic aromatic structures. The electron donors are used in a combination with electron acceptor molecules that are in general substituted fullerenes (e.g., PCBM)[6,10] or perylene bisimides.[11,12] Recent pump−probe measurements on blends composed of photoexcited conjugated polymers and PCBM show a high electron-transfer efficiency in these species.[13]

The control of the morphology and the formation of an interpenetrating donor−acceptor network by phase separation is of great importance for the device properties.[14] However, this is a very difficult task in a blend of two different components.[15] An alternative might be the use of donor−acceptor hybrid molecules in which the intramolecular electron transfer can occur with high efficiency.[16,17] In solar cells of such materials,

Received: August 29, 2011
Revised: October 4, 2011
Published: October 17, 2011

fast recombination processes usually prevent the extraction of the separated charges.[18,19] However, structural order that results in a fast extraction of the emerging charges is discussed as a way to avoid these recombination processes.[20] Therefore, several attempts have been undertaken with the aim to synthesize molecules that aggregate into well-defined donor−acceptor superstructures.[16,21] Shape-persistent macrocycles with an interior in the nanometer regime are interesting compounds for the use in organic photovoltaics because their rigidity allows a defined positioning of functional side groups.[22]

In this work, we investigate a recently synthesized shape-persistent planar macrocyclic donor−acceptor hybrid molecule that can undergo a photoexcited charge separation and that allows a columnar arrangement to minimize charge recombination. The electron donor is part of the macrocycle backbone, and two electron acceptors are present as extra-annular side groups that are covalently bound to the periphery of the rings. The phenylene-bithiophene macrocycle **1** as well as the donor−acceptor hybrid molecule **3** (Figure 1) were synthesized by oxidative coupling of two thiophene-terminated half-ring precursor molecules under pseudo high dilution conditions.[22,23]

We investigate the paramagnetic charge-separated state of the donor−acceptor hybrid by continuous wave (cw) and electron-spin echo (ESE) detected EPR measurements. Long-lived charge-separated states in similar donor−acceptor hybrids have previously been directly measured by electron paramagnetic resonance (EPR) techniques, and two well-resolved EPR signals belonging to the radical cation of the conjugated polymer and the PCBM radical anion have been identified.[24,25] Charge separation may furthermore lead to the formation of triplet states ($S = 1$) that have been formed from radical pair precursor states. The triplet state is paramagnetic and directly accessible by EPR spectroscopy and provides information about the distribution of the unpaired electrons and their magnetic coupling, called the zero field splitting (ZFS). We note here that the transient radicals, which are formed after optical excitation, can be monitored by the EPR technique on a nanosecond time scale. Faster processes or processes occurring in the excited singlet state cannot be investigated by magnetic resonance techniques and have to be complemented by fast optical techniques. The experiments are complemented with DFT calculations to analyze the zero field splitting of the observed triplet states, which turns out to be localized either on the donor (**1**) or on the acceptor (**2**) moieties. The observed radical pair states induced upon illumination are promising with respect to using this type of stackable organic donor−acceptor hybrid molecules in organic photovoltaic cells.

MATERIALS AND METHODS

Sample Preparation and UV/Vis Spectroscopy. The concentration of **1** and **2** in THF (distilled prior to use to remove the stabilizing agent) was 1 mM for each component. The concentration of **3** was 1 mM in THF. The thiophene macrocycle **1** has an absorption maximum at 380 nm; additionally, a significant absorption is present at 430 nm. The perylene bisimide dye **2** has a significant absorption at 480 and 525 nm. The UV/Vis spectrum of the covalently linked donor−acceptor hybrid molecule **3** has an absorption spectrum that is essentially a linear superposition of absorption spectra of complexes **1** and **2** (see Figure S1 in the Supporting Information).[23] Selective excitation of the donor and acceptor molecules is achieved at excitation wavelengths of 430 and 525 nm, respectively.

EPR Spectroscopy. cw EPR spectra were recorded on a Bruker ESP 300E EPR spectrometer equipped with a 4102ST X-band resonator and an Oxford ESR900 helium gas-flow cryostat. ESE-detected EPR was recorded on a Bruker Elexsys E580 FT EPR spectrometer equipped with a MD4 Q-band EPR/ENDOR resonator and an Oxford CF935 helium gas-flow cryostat. Continuous light excitation was performed with a 150 W Hamamatsu xenon lamp. Laser excitation has been accomplished with a Continuum Surelite OPO Plus laser pumped by a Surelite II Nd:YAG laser at 10 Hz repetition rate. Excitation at 430 nm was performed with 12 mJ/pulse, at 525 nm with 10 mJ/pulse. The cw EPR measurements were carried out at 130 K. The applied microwave frequency for **1**/**2** and **3** were 9.467 and 9.469 GHz, respectively, and the microwave power was 2 mW. To measure the time evolution of the radical signal during light irradiation, the magnetic field was set to the position of maximum EPR signal, and the signal was observed as a function of time.

ESE-detected EPR measurements were performed at Q-band at 10 K. The microwave frequency was typically 34 GHz (Q-band). The pulse sequence for the ESE-detected EPR experiment is shown in Scheme 1. It consists of a laser pulse followed after a delay (delay after flash, DAF) time by two microwave pulses and detection by a Hahn echo. The lengths of the microwave pulses were 36 and 72 ns, respectively, and the delay between the two pulses was 250 ns; the DAF time was variable. The accumulation time was typically 5 min for a cw EPR spectrum and 30 min for an ESE-detected EPR spectrum. ESEEM effects were not observed, in line with the fact that the ESEEM effect for protons is absent at 34 GHz and that of nitrogen in this case is also absent given that the nitrogen atoms of PBI do not carry spin density (vide infra).

DFT Calculations. DFT calculations of the triplet state of **1**, **2**, and **3** were performed with the ab initio, DFT, and semiempirical SCF-MO package ORCA.[26−30] All calculations were performed using the BP86 functional, SVP basis set, and SV/C auxiliary basis set.[31] The convergence criteria for the SCF procedure were 10^{-7} hartree for the change in total energy and 10^{-4} for the DIIS error. The model geometry of **1**, **2**, and **3** was constructed with Gaussview.[32] All atoms were geometry optimized using ORCA. Molecular orbital plots have been constructed using the orca_plot program from the ORCA package and Gaussview.[32] ZFS parameters for the triplet state of **1** and **2** have been calculated with ORCA using spin-unpolarized orbitals. The effect of the spin polarization on ZFS value D has been taken in account for **2** using the method described in ref 33. The spin densities for the HOMO and LUMO have been estimated from additional DFT calculations of the cation and the anion of **2**. For the triplet state, the total spin density amounts to 200%, representative of the two unpaired electrons.

RESULTS

cw EPR Spectra of Light-Induced Radicals. An X-band cw EPR spectrum of a frozen solution of the mixture **1**/**2** measured at 130 K under continuous illumination is shown in Figure 2a. The EPR signal has a width of 0.38 mT and is essentially without hyperfine structure, indicative of a delocalized singly occupied molecular orbital (SOMO) and virtually no spin density at ^{14}N ($I = 1$). Figure 2b shows the evolution of the radical signal during light illumination. The growth of the radical signal has a multiexponential character, with a fast time constant of about 3.7 s and a slow time constant of about 47 s. After switching off the light, the radical signal

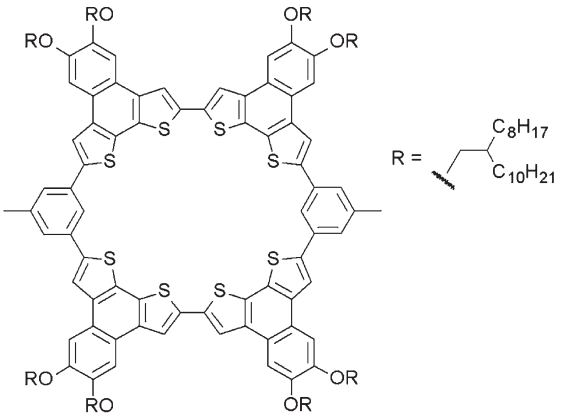

1

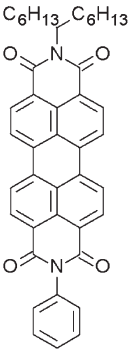

2

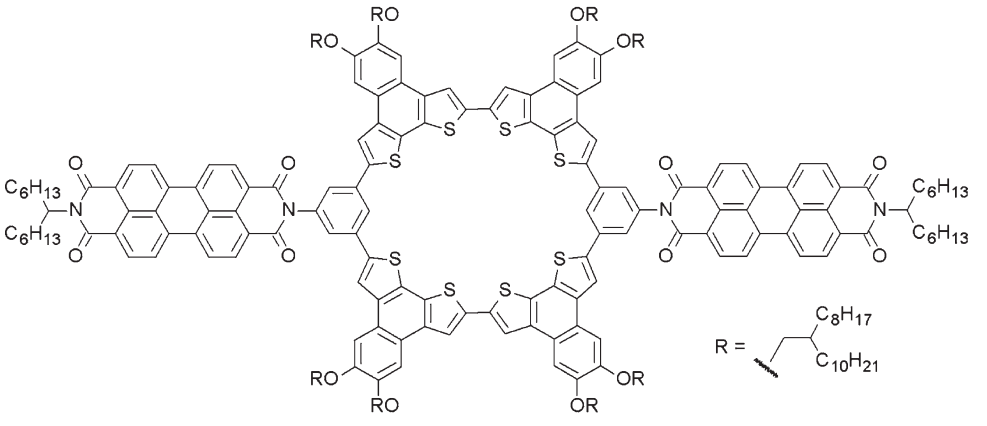

3

Figure 1. Schematic view of the phenylene−bithiophene macrocycle (**1**), perylene bisimide (**2**), and the covalently bound donor−acceptor molecule (**3**).

Scheme 1. Pulse Scheme for the ESE-Detected EPR Experiment

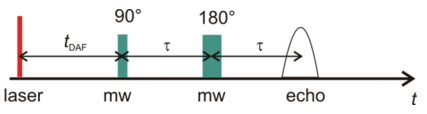

decays with a fast time constant of 4.9 s and a slow time constant of 69 s and reaches 54% of the maximum intensity. Upon thawing the sample to room temperature and cooling again to 130 K, the signal disappears.

The cw EPR spectrum of **3** measured at 130 K under continuous illumination is shown in Figure 2c. The width of the spectrum is 0.51 mT, larger than that of the mixed frozen solution of **1**/**2**. The intensity of the radical signal of complex **3** is significantly smaller than that of **1**/**2**, indicating that the radical pairs are either formed in low quantity or that they recombine quickly. The evolution of the radical signal upon switching

dx.doi.org/10.1021/jp208334y |*J. Phys. Chem. B* 2011, 115, 13526–13533

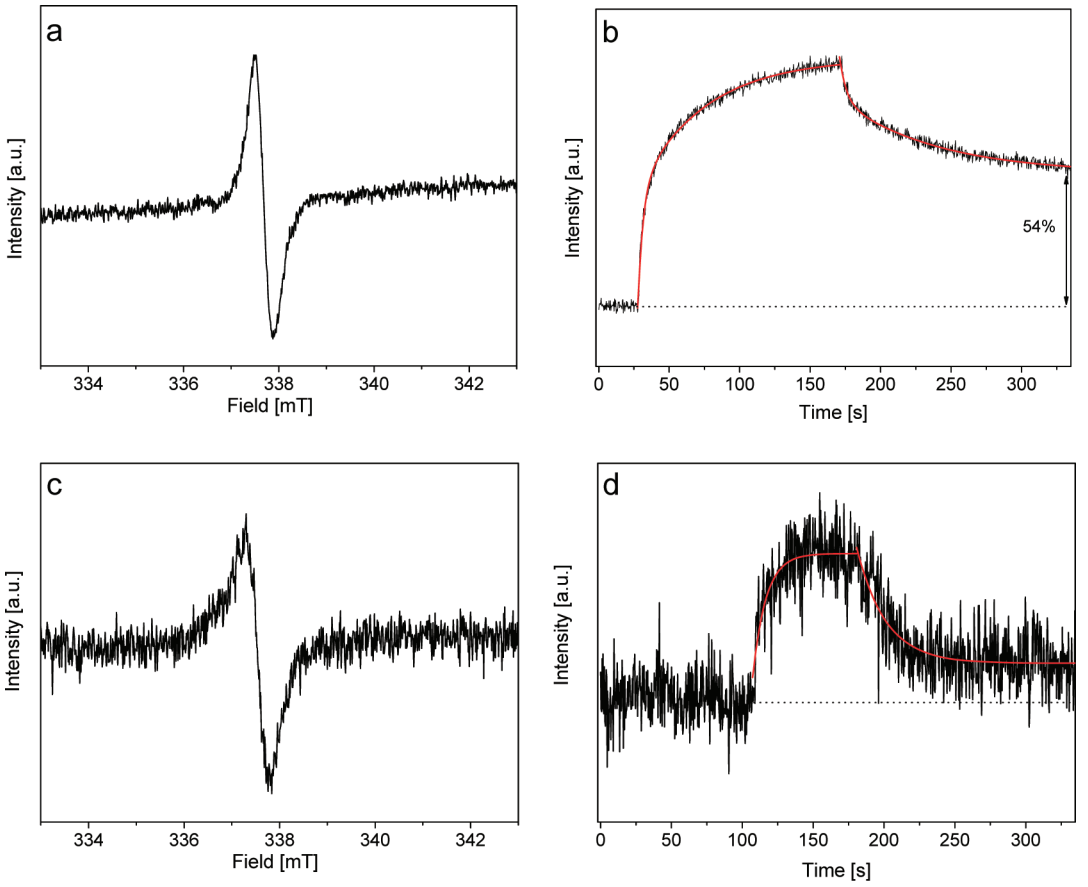

Figure 2. (a) cw EPR spectrum and (b) time evolution of **1**/**2** upon switching on (t = 35 s) and switching off (t = 180 s) the continuous illumination at 130 K in X-band. (c) cw EPR spectrum and (d) time evolution of **3** under the same conditions. The g values in (a) and (c) amount to 2.0036.

on and off the continuous illumination is given in Figure 2d. The growth constant of 10 s is much faster than that for **1**/**2**. The signal decays with a time constant of 20 s after switching off the light, which is also much faster than that for **1**/**2**. The amplitude of the radical signal reaches 25% of the maximum intensity.

ESE-Detected EPR of the Photoinduced Triplet State. The ESE-detected EPR spectrum of **1** upon pulsed laser excitation at 430 nm recorded at 10 K is shown in Figure 3a. The spectrum has a polarization pattern EEEAAA. The D and E values amount to 0.065 and 0.007 cm^{-1}, typical for organic triplet states.[34] Figure 3b shows the ESE-detected EPR spectrum of **2** at 10 K excited at 525 nm. The spectrum again has the polarization pattern EEEAAA. The D and E values are significantly smaller than those for **1** and amount to 0.044 and 0.004 cm^{-1}. The signals, marked with an asterisk, are present in the center of the spectra; they belong to a photoaccumulated stable radical.

The ESE-detected EPR spectra of **1**/**2** recorded at 10 K with excitation at 430 and 525 nm are shown in Figure 3c and d, respectively. The spectrum at 525 nm is characterized by a polarization pattern EEEAAA; the spectrum at 430 nm contains eight transitions, indicative of the presence of more than one triplet state. Nevertheless, the major features of the spectrum indicate D and E values for **1**/**2** identical to those for **1**. At 525 nm, the ZFS parameters D and E amount to D = 0.044 cm^{-1} and E = 0.004 cm^{-1}, identical to that of **2**. Interestingly, upon careful examination, the triplet EPR spectra of **1**/**2** are more symmetric around the center of the spectrum than the spectra for **1** and **2**. This is reflected in the g_x and g_y values, which are slightly larger for **1** and **2** than for **1**/**2** (vide infra).

Figure 3e shows the ESE-detected EPR spectrum of complex **3** in frozen solution at 525 nm excitation recorded at 10 K in Q-band. The spectrum has the polarization pattern AEEAAE, which is different from that observed in the frozen solution of **1**/**2**. The D and E values have been read from the spectrum and amount to D = 0.044 cm^{-1} and E = 0.004 cm^{-1}, again identical to those for **2**. With excitation at 430 nm, the ESE-detected EPR spectrum of **3** is identical to that excited at 525 nm. In the center region of the ESE-detected EPR spectra of **3**, additional features with polarization pattern EAAEEA are visible (see Figure S2 in the Supporting Information).

DAF experiments have been performed for **3**, and time constants of growth and decay of the triplet signal and transient signal have been measured. The amplitude of the triplet EPR signal grows with a field-independent time constant of 1.7 μs, whereas the transient signal grows with a time constant of 200 ns (see Figure S3 in the Supporting Information). The decay of the triplet signal to the ground state occurs with a time constant of about 133 μs depending on the field position.

DFT Calculations. The HOMO and LUMO orbitals from DFT calculations for **1**, **2**, and **3** are shown in Figure 4a−c, respectively. The DFT calculations for **1** show a delocalized electron spin density at the carbon atoms of the phenylene−bithiophene macrocycle. The spin density at the carbon atoms of the ring amounts to 5−6% on each carbon atom. The spin density at the carbon atoms that belong to rings A and B (see

dx.doi.org/10.1021/jp208334y |J. Phys. Chem. B 2011, 115, 13526–13533

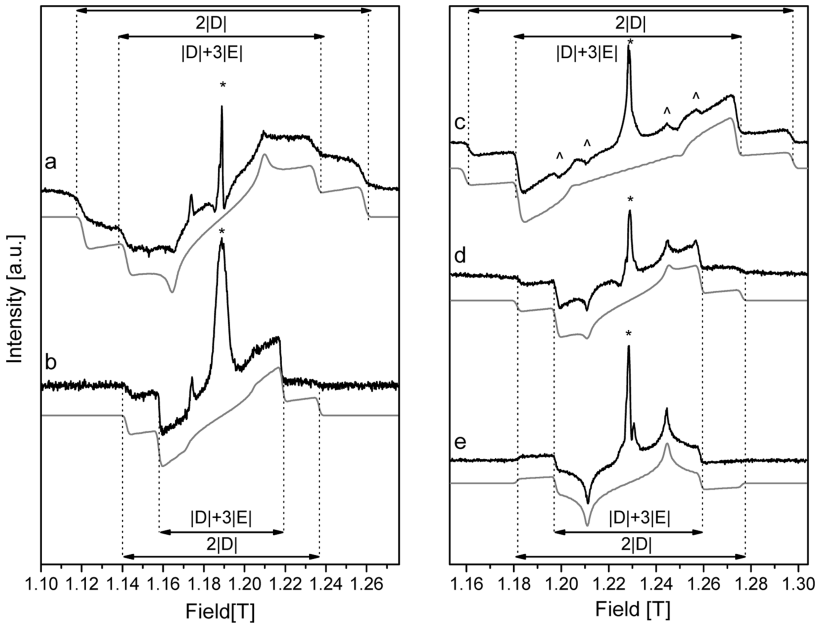

Figure 3. ESE-detected EPR spectra measured at Q-band at 10 K (upper traces) and simulations (lower traces): (a) **1**, 430 nm, t_{DAF} = 0.5 μs; (b) **2**, 525 nm, t_{DAF} = 0.5 μs; (c) mixture **1**/**2**, 430 nm, t_{DAF} = 0.5 μs; (d) mixture **1**/**2**, 525 nm, t_{DAF} = 0.5 μs; (e) **3**, 525 nm, t_{DAF} = 4 μs. The signals marked with "*" stem from a photoaccumulated radical signal that persists upon switching off the illumination. The microwave frequency for (a) and (b) is 33.3419 GHz, and for (c)−(e) is 34.4280 GHz.

Figure 4a) amounts to about 6.5% on each carbon atom. The LUMO of **1** contains significant spin density of 2.2% on each sulfur atom. The HOMO and LUMO of **2** are evenly distributed over the carbons and oxygen atoms. Spin density at the nitrogen atoms is absent. For **3**, the HOMO is essentially identical to that of **1**. Interestingly, the LUMO is doubly degenerate and constitutes a set of two orbitals identical to that of **2** and localized on either PBI moiety. Because the LUMO is doubly degenerate, any linear combination within this set thus also constitutes a valid LUMO.

The D and E values for **1** deduced from DFT calculations (D = 0.179 cm^{-1}, E = 0.044 cm^{-1}) differ significantly from the experimental values of 0.065 and 0.0075 cm^{-1} for D and E, respectively. The ZFS parameter D of **1** is determined largely by spin−orbit coupling, which seems to be overestimated in the DFT calculations. The calculated D and E values for **2** (D = 0.026 cm^{-1}, E = 0.006 cm^{-1}) are in better agreement with the experimental values. If spin polarization is taken into account,[33,35] the calculated D value amounts to 0.035 cm^{-1}, which is in reasonable agreement with the experiment.

DISCUSSION

Light-Induced Radicals. The cw EPR spectra both of **1**/**2** and of complex **3** show the formation of radical signals during light irradiation, albeit with low intensity. In particular, the formation of radical signals indicates that light-induced charge separation occurs both in **1**/**2** and **3**. The time constants are on the time scale of several seconds, which implies that this process corresponds to *intermolecular* charge separation. Because the lifetime of the radical in **3** is shorter than that in **1**/**2**, the charge recombination in frozen solution in **3** apparently proceeds more rapidly, possibly indicating a larger electronic interaction between the molecules **3** as compared to the mixture **1**/**2**.

ESE-Detected EPR of the Triplet State. By EPR investigation of the triplet state, information can be obtained about *intramolecular* charge separation. Before we discuss the EPR spectra of the triplet state, it is important to realize that multiple mechanisms of triplet formation exist. These mechanisms give rise to different absorptive and emissive polarization patterns. Vice versa, analysis of the polarization patterns provides direct information about the presence of radical pair precursor states related to intramolecular charge separation. The first and most common mechanism of triplet formation is called intersystem crossing (ISC). In this mechanism, the excited electron does not leave the excited molecule. Spin-dependent processes, in particular spin−orbit (SO) coupling,[28] flip the spin of one of the unpaired electrons, thereby forming the triplet state. For the ISC mechanism, the population p_i of the $M_S = i$ sublevels is distributed over the three triplet sublevels according to[36]

$$p_i = \sum_{u=x,y,z} c_{iu}^2 p_u \qquad (1)$$

where $i = -1, 0, +1$, the coefficients c_{iu} represent the mixing of the zero field states in the magnetic field, and p_u ($u = x, y, z$) is the population of one of the three zero-field sublevels.[36]

The triplet state can be also formed via a radical pair (RP) mechanism.[37] In this mechanism, the excited electron is transferred from the donor to the acceptor and forms a radical pair state $D^{\bullet+}A^{\bullet-}$ (Figure 5a). The radical pair state is initially present as a singlet state. In the presence of a magnetic field, the singlet state remains degenerate only with the T_0 sublevel of the triplet radical pair state. A significant mixing of the S and T_0 levels occurs, in which the radical pair states oscillate back and forth between S and T_0. The T_0 radical pair state can then recombine to form the triplet state T_1 of the acceptor (Figure 5a). In this mechanism, the M_S = 0 sublevel of ^{3}A is exclusively populated (Figure 5b). This implies that shortly after the laser flash and

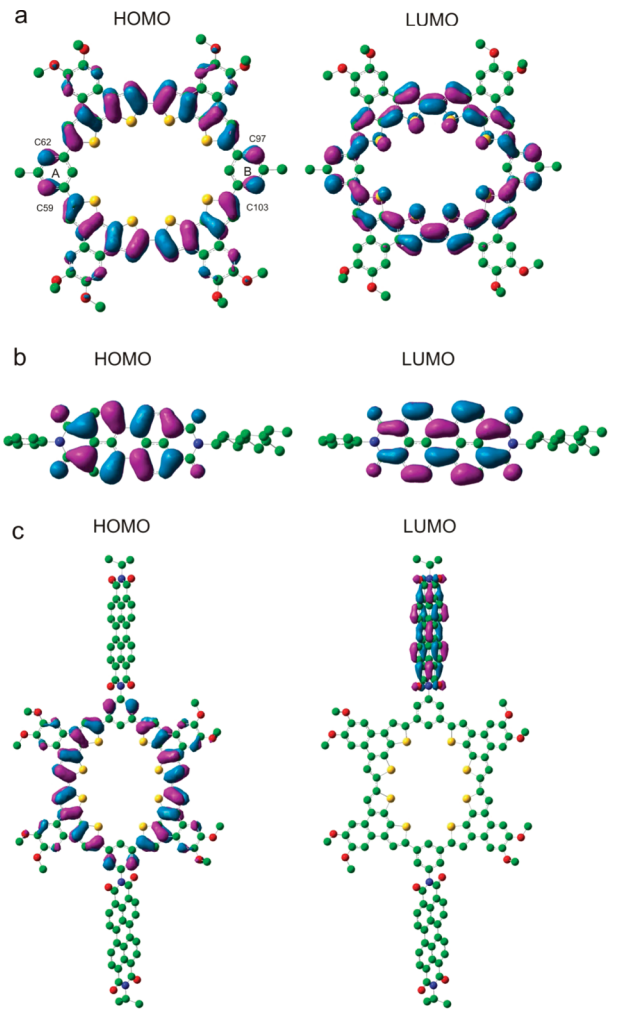

Figure 4. HOMO and LUMO orbitals from DFT calculations of (a) **1**, (b) **2**, and (c) **3**.

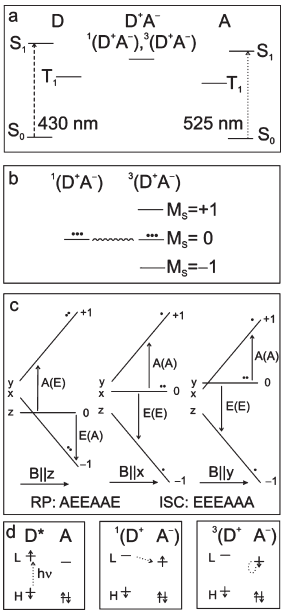

Figure 5. (a) Energy level diagram (state energies) for electron transfer and charge separation in **3**. After excitation at 430 or 525 nm, a charge-separated state $D^{\bullet+}A^{\bullet-}$ is formed. If the charge-separated state lives longer than 10 ns, the spin of either unpaired electron may flip and selectively populates the $M_S = 0$ level of the triplet radical pair state, as indicated in (b). This state decays to the triplet state (T_1) of the acceptor, thus selectively populating the $M_S = 0$ level of T_1, giving rise to an AEEAAE polarization pattern as given by the arrows in (c), whereas an ISC triplet would give EEEAAA, indicated in brackets in (c) and with the population represented by closed circles. A corresponding MO picture for radical pair formation is given in (d). H indicates the HOMO, L the LUMO, D the donor (**1**), and A the acceptor (**2**).

before decay processes play a role, all $T_0 \rightarrow T_{+1}$ transitions are absorptive and $T_0 \rightarrow T_{-1}$ are emissive (Figure 5c). If the zero-field parameter D is positive, a polarization pattern AEEAAE is observed for the triplet state formed via radical pair mechanism. By ISC, this particular polarization pattern is impossible.

The ISC crossing triplet spectra have been simulated by implementation of eq 1, with p_x, p_y, and p_z being the input parameters, and an orientational averaging procedure to simulate the frozen solution. In this case, the amplitude of the EPR signal is taken to be proportional to the population differences of the triplet sublevels. For the simulation of the radical pair triplet spectra, the $M_S = 0$ level is assigned a population of 1.0, irrespective of the orientation of the ZFS principal axes with respect to the direction of the magnetic field. The EPR spectra of all compounds in the triplet state have been successfully simulated by either an ISC or a radical pair mechanism. The simulations reproduce the positions of essentially all bands in the spectra as well as the overall line shape.

The EPR spectrum of **1** is successfully simulated by an ISC mechanism of triplet formation. The simulation is included in Figure 3a, and the simulation parameters are given in Table 1. The triplet sublevels T_x and T_y are equally populated, whereas T_z is empty. This gives rise to a polarization pattern EEEAAA (Figure 5c). Similarly, the EPR spectrum of **2** is also simulated under assumption of an ISC mechanism of the triplet formation. The simulation is shown in Figure 3b. **2** is characterized by a smaller ZFS parameter D, and the population of the triplet sublevels is slightly different from that in **1**. The presence of only a small fractional population p_z is indicative of a $\pi \rightarrow \pi^*$ excitation of the respective molecule. At Q-band, a small g anisotropy is necessary to correctly simulate the spectra, because the fields of resonance for the X and Y canonical orientations are not centered around the free electron g value.

The D and E values of **1**/**2** used in the simulation of the Q-band ESE-detected EPR spectra measured at 430 and 525 nm (Figure 3c and d, respectively) are identical to those of **1** and **2**, respectively. This is expected, because the molecules are not covalently bound, and the orbitals remain localized on either molecule. Nevertheless, the intensity has redistributed, and the polarization pattern in Figure 3c has changed to EEAEAA. Moreover, although irradiation at 430 nm mainly excites the electron donor **1**, the electron acceptor **2** may also be excited, giving rise to spectral features marked with ˆ in Figure 3c. At 525 nm, only **2** is excited. The observation of a redistribution of intensity in **1**/**2** as compared to **1** and **2** indicates that additional interactions occur between the two constituents in the mixture, which affect the spin orbit coupling. The spectrum in Figure 3c has been successfully simulated by an ISC mechanism, albeit with slightly changed fractional populations of the ZFS sublevel (cf., Table 1). The triplet spectrum indicates that no electron transfer from donor to acceptor on the time scale of nanoseconds

dx.doi.org/10.1021/jp208334y |*J. Phys. Chem. B* 2011, 115, 13526–13533

Table 1. ZFS Parameters D and E for 1, 2, Mixture 1/2, and the Covalently Bound 3 As Obtained from Simulations of the EPR Spectrum Measured with Laser Excitation at Wavelength λ_{exc}[a]

	1	1/2	2	1/2	3
λ_{exc} [nm]	430	430	525	525	525
D [cm^{-1}]	0.0645	0.0645	0.0442	0.0442	0.0442
E [cm^{-1}]	0.0075	0.0075	0.0043	0.0043	0.0043
p_x	0.50	0.30	0.35	0.40	0.60
p_y	0.50	0.60	0.50	0.55	0.30
p_z	0.00	0.10	0.15	0.05	0.10
g_x	2.0060	2.0030	2.0050	2.0030	2.0035
g_y	2.0040	2.0030	2.0050	2.0030	2.0030
g_z	2.0025	2.0025	2.0025	2.0025	2.0025

[a] Also indicated are the populations p_x, p_y, and p_z for the ISC mechanism and the three canonical g values. The linewidth used in all simulations amounts to 0.8 mT.

occurs in **1**/**2** after excitation of the donor molecule. The g-tensor anisotropy has reduced with respect to that of **1** and **2**, which may also be a consequence of possible contact between nearby molecules in the frozen solution of **1**/**2**.

In analogy to **2**, the EEEAAA polarization pattern of the EPR spectrum of **1**/**2** at 525 nm (Figure 3d) seems to be characteristic for a triplet state formed by ISC mechanism. Surprisingly, although the same D and E parameters as for **2** are required for the simulation, the intensity distribution of the EPR spectrum cannot be reproduced solely by ISC (simulation given in the Supporting Information). Under assumption of 90% ISC and 10% RP mechanisms, the triplet EPR spectrum of **1**/**2** excited at 525 nm is successfully simulated. The simulation parameters are given in Table 1. It may be possible that an electron is transferred from the doubly occupied HOMO of **1** to the, after excitation, singly occupied HOMO of **2** via HOMO-based electron transfer.[38,39] Thus, a radical pair TPH$^{\bullet+}$PBI$^{\bullet-}$ is again formed, followed by the formation of the triplet state via the radical pair mechanism (Figure 5a).

Interestingly, the Q-band ESE-detected EPR spectrum of complex **3** shown in Figure 3e does not depend on the excitation wavelength. The polarization pattern AEEAAE and shape of the EPR spectrum of **3** are more characteristic for a RP mechanism than for an ISC mechanism (cf., Figure 5c), and the growth constant (1.7 μs) is uniform over the entire magnetic field range. The EPR spectrum is simulated well under assumption of 45% RP and 55% ISC mechanisms, which apparently coexist (cf., Figure 3e and the Supporting Information). By excitation of the molecule at 430 nm, the excited electron is transferred from the LUMO of TPH to the LUMO of PBI and forms a radical pair TPH$^{\bullet+}$PBI$^{\bullet-}$ (Figure 5d). Simultaneously, HOMO-based electron transfer can proceed from the donor to the acceptor by excitation at 525 nm to form the same radical pair state TPH$^{\bullet+}$PBI$^{\bullet-}$. The radical pair state then decays, first into the triplet state of the donor. The triplet excitation is subsequently transferred by triplet−triplet energy transfer to the acceptor moiety. Evidence for HOMO-based electron transfer is present in the form of a narrow transient signal in the center of the spectrum at short DAF times after excitation at 525 nm, which is essentially identical to the narrow transient signal observed at 430 nm (see the Supporting Information). The presence of a significant amount of triplet state formed from a radical pair precursor indicates a high probability of intramolecular electron transport and charge separation in this novel donor−acceptor system. A radical pair precursor state is also inferred from the DFT calculations of **3**, where the HOMO is located at TPH and the LUMO at PBI.

CONCLUSION

In this work, a systematic EPR study of a macrocyclic donor−acceptor hybrid has been performed. Using cw EPR spectroscopy at 9.5 GHz with continuous light excitation of the mixture of the molecular compounds **1** and **2** and the covalently linked hybrid **3**, radicals have been detected and analyzed. A radical signal forms during continuous light illumination of the systems **1**/**2** and **3**. The lifetime of the radicals on the time scale of several seconds is an indication for long-lived *intermolecular* charge separation, which occurs with low yield.

ESE-detected EPR spectroscopy on the triplet state at 34 GHz using laser excitation has been used for the detection of *intramolecular* charge-separated states. The triplet state of the acceptor is formed after excitation of either the donor or the acceptor in **3**. In total, 45% of the triplet state is formed via a TPH$^{\bullet+}$PBI$^{\bullet-}$ radical pair precursor state by either LUMO-based or HOMO-based electron transfer depending on the excitation wavelength. This is further confirmed by DFT calculations in which the HOMO of **3** is found at TPH and the LUMO is found at PBI.

ASSOCIATED CONTENT

Supporting Information. UV/vis spectra of **1**, **2**, and **3**; ESE-detected triplet EPR spectra of **3** at 430 and 525 nm excitation measured at T = 10 K at Q-band; ESE-detected EPR spectra of **3** at 10 K recorded at different times after laser flash; simulation of EPR spectra of **1**/**2** and **3** at 525 nm using pure ISC and RP mechanisms; and Cartesian coordinates of **1**, **2**, and **3** used in the DFT calculations. This material is available free of charge via the Internet at http://pubs.acs.org.

AUTHOR INFORMATION

Corresponding Author

*Phone: ++49 228 73 2919. Fax: ++49 228 73 2551. E-mail: vgastel@pc.uni-bonn.de.

Present Addresses

[§]Max Planck Institute for Bioinorganic Chemistry, Stiftstrasse 34-36, D-45470 Mülheim an der Ruhr, Germany.

ACKNOWLEDGMENT

This project is financially supported by the Deutsche Forschungsgemeinschaft (DFG), SFB 813, and by the University of Bonn.

LIST OF ABBREVIATIONS

A, acceptor
cw, continuous wave
D, donor
DAF, delay after flash
DFT, Density Functional Theory
DIIS, direct inversion of iterative subspace
EPR, electron paramagnetic resonance

ESEEM, electron spin echo envelope modulation
HOMO, highest occupied molecular orbital
ISC, intersystem crossing
LUMO, lowest unoccupied molecular orbital
MO, molecular orbital
OPO, optical parametric oscillator
PBI, perylenebisimide
RP, radical pair
SCF, self-consistent field
SO, spin−orbit
TPH, thiophene
UV, ultraviolet
ZFS, zero field splitting

REFERENCES

(1) Markvart, T. *Solar Electricity*; Wiley: Chichester, 2000.
(2) Brabec, C. J.; Dyakonov, V.; Parisi, J.; Sariciftci, N. S. *Organic Photovoltaics: Concept and Realizations*; Springer Verlag: Berlin, Heidelberg, 2003.
(3) Höger, S.; McNamara, J. J.; Schricker, S.; Wudl, F. *Chem. Mater.* **1994**, *6*, 171–173.
(4) Green, M. A.; Emery, K.; Hishikawa, Y.; Warta, W. *Prog. Photovoltaics* **2011**, *19*, 84–92.
(5) Clarke, T. M.; Durrant, J. R. *Chem. Rev.* **2010**, *110*, 6736–6767.
(6) Sariciftci, N. S.; Smilowitz, L.; Heeger, A. J.; Wudl, F. *Science* **1992**, *258*, 1474–1476.
(7) Janssen, R. A. J.; Moses, D.; Sariciftci, N. S. *J. Chem. Phys.* **1994**, *101*, 9519–9527.
(8) Janssen, R. A. J.; Christiaans, M. P. T.; Pakbaz, K.; Moses, D.; Hummelen, J. C.; Sariciftci, N. S. *J. Chem. Phys.* **1995**, *102*, 2628–2635.
(9) Janssen, R. A. J.; Hummelen, J. C.; Lee, K.; Pakbaz, K.; Sariciftci, N. S.; Heeger, A. J.; Wudl, F. *J. Chem. Phys.* **1995**, *103*, 788–793.
(10) Morita, S.; Zakhidov, A. A.; Yoshino, K. *Solid State Commun.* **1992**, *82*, 249–252.
(11) Würthner, F.; Chen, Z. J.; Hoeben, F. J. M.; Osswald, P.; You, C. C.; Jonkheijm, P.; von Herrikhuyzen, J.; Schenning, A. P. H. J.; van der Schoot, P. P. A. M.; Meijer, E. W.; Beckers, E. H. A.; Meskers, S. C. J.; Janssen, R. A. J. *J. Am. Chem. Soc.* **2004**, *126*, 10611–10618.
(12) Höger, S. *J. Polym. Sci., Part A: Polym. Chem.* **1999**, *37*, 2685–2698.
(13) Brabec, C. J.; Zerza, G.; Cerullo, G.; de Silvestri, S.; Luzzati, S.; Hummelen, J. C.; Sariciftci, S. *Chem. Phys. Lett.* **2001**, *340*, 232–236.
(14) Rosselli, S.; Ramminger, A. D.; Wagner, T.; Lieser, G.; Höger, S. *Chem.-Eur. J.* **2003**, *9*, 3481–3491.
(15) Brabec, C. J.; Heeney, M.; McCulloch, I.; Nelson, J. *Chem. Soc. Rev.* **2011**, *40*, 1185–1199.
(16) Cravino, A.; Sariciftci, N. S. *J. Mater. Chem.* **2002**, *12*, 1931–1943.
(17) Roncali, J. *Chem. Soc. Rev.* **2005**, *34*, 483–495.
(18) Bottari, G.; de la Torre, G.; Guldi, D. M.; Torres, T. *Chem. Rev.* **2010**, *110*, 6768–6816.
(19) Segura, J. L.; Martin, N.; Guldi, D. M. *Chem. Soc. Rev.* **2005**, *34*, 31–47.
(20) Nishizawa, T.; Lim, H. K.; Tajima, K.; Hashimoto, K. *Chem. Commun.* **2009**, 2469–2471.
(21) Fischer, M.; Lieser, G.; Rapp, A.; Schnell, I.; Mamdouh, W.; de Feyter, S.; de Schryver, F. C.; Höger, S. *J. Am. Chem. Soc.* **2004**, *126*, 214–222.
(22) Höger, S. *Chem.-Eur. J.* **2004**, *10*, 1320–1329.
(23) Maier, S. K.; Jester, S.-S.; Müller, U.; Müller, W. M.; Höger, S. *Chem. Commun.* **2011**, *47*, 11023–11025.
(24) Allemand, P. M.; Srdanov, G.; Koch, A.; Khemani, K.; Wudl, F.; Rubin, Y.; Diederich, F.; Alvarez, M. M.; Anz, S. J.; Whetten, R. L. *J. Am. Chem. Soc.* **1991**, *113*, 2780–2781.
(25) Dyakonov, V.; Zoriniants, G.; Scharber, M.; Brabec, C. J.; Janssen, R. A. J.; Hummelen, J. C.; Sariciftci, N. S. *Phys. Rev. B* **1999**, *59*, 8019–8025.
(26) Ganyushin, D.; Neese, F. *J. Chem. Phys.* **2006**, *125*, 024103.
(27) Neese, F. *ORCA - An ab initio, Density Functional and Semi-empirical Program Package*; Universität Bonn: Bonn, Germany, 2011.
(28) Neese, F. *J. Am. Chem. Soc.* **2006**, *128*, 10213–10222.
(29) Neese, F.; Solomon, E. I. *Inorg. Chem.* **1998**, *37*, 6568–6582.
(30) Neese, F. *J. Chem. Phys.* **2003**, *118*, 3939–3948.
(31) Schäfer, A.; Horn, H.; Ahlrichs, R. *J. Chem. Phys.* **1992**, *97*, 2571–2577.
(32) Dennington, R., II; Keith, T.; Eppinnett, K.; Hovell, W. L.; Gilliland, R. *Gaussview*; Semichem, Inc.: 2003.
(33) van Gastel, M. *J. Chem. Phys.* **2009**, *131*, 124111.
(34) Atherton, N. *Principles of Electron Spin Resonance*; Ellis Horwood PTR Prentice Hall: New York, 1993.
(35) McConnell, H. M.; Chesnut, D. B. *J. Chem. Phys.* **1958**, *28*, 107–117.
(36) Dauw, X. L. R.; Poluektov, O. G.; Warntjes, J. B. M.; Bronsveld, M. V.; Groenen, E. J. J. *J. Phys. Chem. A* **1998**, *102*, 3078–3082.
(37) Hore, P. J. Analysis of polarized EPR spectra. In *Advanced EPR in Biology and Biochemistry*; Hoff, A., Ed.; Elsevier: Amsterdam, 1990; pp 405−440.
(38) Allen, G. C.; Hush, N. S. *Inorg. Chem.* **1967**, *6*, 4–15.
(39) Marchanka, A.; Paddock, M.; Lubitz, W.; van Gastel, M. *Biochemistry* **2007**, *46*, 14782–14794.